MEASUREMENT SCIENCE REVIEW, **20**, (2020), No. 4, 162-170

sciendo

ISSN 1335-8871

MEASUREMENT SCIENCE REVIEW

Journal homepage: https://content.sciendo.com

Active Vision Reconstruction Based on Ratio Invariability of Triangle Areas Generated from Triangle Array in Affine Space

Guan Xu[1], Hui Shen[1], Xiaotao Li[2]

[1]*Department of Vehicle Operation Engineering, Transportation College, Nanling Campus, Jilin University, Renmin Street 5988#, 130025, Changchun, Jilin, P. R. China*

[2] *School of Mechanical and Aerospace Engineering, Nanling Campus, Jilin University, Renmin Str. 5988#, 130025, Changchun, Jilin, P. R. China, lixiaotao@jlu.edu.cn*

An active-vision process is presented by the affine invariability of the ratio of triangle areas to reconstruct the 3D object. Firstly, a plate with the triangle array is designed in the same plane of the planar laser. The image of the plate is rectified from the projection space to the affine space by the image of the line at infinity. Then the laser point and the centroids of the triangles constitute a new triangle that bridges the affine space and the original Euclidean space. The object coordinates are solved by the invariant of the triangle area ratio before and after the affine transformation. Finally, the reconstruction accuracy under various measurement conditions is verified by experiments. The influence analyses of the number of line pairs and the accuracy of the extracted point pixels are provided in the experimental results. The average reconstruction errors are 1.54, 1.79, 1.90, and 2.46 mm for the test distance of 550, 600, 650, and 700 mm, which demonstrates the application potential of the approach in the 3D measurement.

Keywords: Active vision, affine invariant, area ratio, triangle array, affine space.

1. INTRODUCTION

Spatial point is the main object in the non-touch applications that deal with the geometrical-value measurement such as part manufacturing [1], [2], traffic guidance [3], [4], scene reconstruction [5], [6], robot control [7], [8], and medical inspection [9], [10]. In the vision-based reconstruction of the 3D point, a camera is a widely used instrument to profile the shape of the 3D object. However, the mapping from the 3D point to the 2D point is a non-invertible process due to the degree loss. Thus, an additional camera is employed for the passive vision reconstruction [11], or an additional structured light is employed for the active vision reconstruction [12].

The stereo vision consists of two cameras [13]. The key of the stereo vision is matching the corresponding points between two images of two cameras. The geometrical constraint of pole-polar-line relationship is often adopted to solve the problem [14]. The active vision is structured by a light source and a camera. The light source generates the line pattern [15], planar pattern [16], or coded pattern [17], etc. The line pattern light takes the advantage of the simplicity to be processed for the reconstruction and the disadvantage of little information. The coded pattern light benefits the construction by the abundant information, whereas the coded pattern tends to be affected by the environmental light. The planar pattern is a moderate configuration as it provides relatively abundant information and is relatively impervious to the environmental light influence.

Previous studies focused on the object reconstruction from the camera image with the vanishing point, which is the mapping of the point at infinity. The projection structure of the camera model is simplified, and then the intrinsic and extrinsic parameters are derived from the image features. Orghidan et al. [18] present a self-calibration method for the structured light with the vanishing points. The projector keystone effect is removed by the vanishing points. Then the chessboard-pattern structured light is mapped to a simple planar surface to calibrate the camera-projector system. The method felicitously applies the projector to generate the chessboard pattern on a non-pattern surface that replaces the patterned target for the calibration. Nevertheless, the assumptions of the principle point on the image center and two vanishing points are required for the reconstruction. E. Guillou et al. [19] propose a camera calibration method with the vanishing points for the preliminary 3D reconstruction from the single image. Two pairs of vertical lines are the necessary pattern on the 2D target. The vanishing points are modeled to calculate the focal length and the rotation representation of the camera. The translation representation

DOI: 10.2478/msr-2020-0020

of the camera is derived from the known length of the line segment on the target. The enhancement of the method lies in realizing the camera calibration and the coarse object reconstruction by only one image. But the configuration of two pairs of vertical lines is obligatory in the image, and the principle point is also supposed on the image center. L. Wang et al. [20] provide a camera calibration method based on the vanishing line. A hexagon is used as the calibration target. First, the vanishing line is calculated according to the projection image. The azimuths are calculated according to the relevant information from the vanishing line. Finally, the camera position parameters are calibrated by the geometric projection relationship. The method simplifies the process of image feature extraction, whereas at least three pairs of the parallel lines are necessary for the hexagon. Y. Zhao et al. [21] introduce a method to calculate the vanishing line and perform the camera self-calibration by using the circles and the centroids. The image coordinates of the circles are extracted from more than three images. As the vanishing line and the circle center represent the relationship between the polar line and the pole, three linear equations are obtained to calculate the vanishing line. Then the intrinsic parameters are determined by the properties of the circular points. The method is easy to be performed and simple in principle. However, the method requires the camera to take images of the template in three or more different orientations. J. A. Gibbs et al. [22] proposed a three-dimensional vegetation reconstruction method based on active vision. The combination of a robot-arm and a camera realize the dynamic manipulation of the camera viewpoint, which solves the problem of obstacle occlusion in the detection. The view sphere formed by the robot-arm positions the camera. The active vision system ensures the information acquisition of the important morphological structure of the target plant. Finally, the characteristics of the objective plants can be restored automatically by the system. D. S. Schacter et al. [23] proposed a method of the dynamic camera orientation selection based on active vision. The cameras are reconfigurable to capture the deformation of the object with the special points on it. The system obtains the pose information of the moving target. The reconstruction error is minimized by considering the deformation of the object. The experimental results show that the method is more flexible and accurate than the fixed camera system.

As the homography from the reference plane in space to the image contains 9 unknown variables, there are 8 degrees of freedom (DOFs) to be determined for the homography, except for the global scale factor. The 8 DOFs include 3 DOFs of the Euclidean transform, 1 DOF of the similarity transform, 2 DOFs of affine transform, and 2 DOFs of the special projection transform, in the transform order from the reference plane to the image. Most studies solve the 8 DOFs of the homography with geometrical elements on the 2D reference and then depict the features on the 2D reference plane. However, the 8 DOFs are unnecessary to be all solved for the reconstruction purpose theoretically. The image with the geometric distortion derived from the projectivity can be rectified to the image with the affine transform by solving the 2 DOFs of the special projection transform [24]. After the rectification, there is only the affine distortion from the 2D reference plate to the image plane.

In the reconstruction process, the test system including a planar laser, a 2D reference textured by the array of triangles and a camera is constructed to recover the feature of the tested object in Euclidean space. The planar laser is coplanar to the 2D reference plate. A reconstruction method with the active vision is proposed in the affine-distortion-image space, which is based on the affine invariability of the area ratio between the triangle on the reference plane and the triangle consisting of the unknown laser point and centroids of 2 small triangles on the reference plane. The first benefit of the reconstruction method is that the information recovery of the laser projection in Euclidean space is achieved in the affine-distortion-image space. Only 2 unknown DOFs should be solved for the rectification from the projection space to the affine space, which is more convenient and simpler than solving the 8 unknown DOFs from the projection space to the original Euclidean space. The second benefit of the reconstruction method is that the laser projection is recovered by the affine invariability of the area ratio between the triangle on the reference and the triangle with the laser projection. One point of the triangle is the laser point. The other two points of the triangle are generated from two centroids of two small triangles on the reference, which are accurate as the centroid presents the center position calculated by the vertex average value of the small triangle. This method makes full use of the affine invariance of the triangle area ratio to transform the projection-space image with the metrical laser projections into the affine space for the object reconstruction. Two DOFs of the image are necessary to be solved in the affine space, compared with the eight DOFs to be solved of the previous methods. Therefore, the number of degrees to be solved is reduced in the affine space. Moreover, the triangle-array pattern used in this paper not only constructs the affine invariant of the area ratio in the process of reconstruction, but also provides the convenience for the corner detection in image processing.

The rest of the paper is structured as follows. Section 2 constructs the recovery process of the active-vision-method based on the invariability of the ratio of the triangle areas in the affine space. Section 3 verifies the recovery method by the reconstruction experiments and comparison experiments with the benchmark. Section 4 concludes the paper.

2. RECOVERY MODEL

A. System setup

The recovery system is comprised of a planar laser generator, a planar reference with the triangle array pattern, and a camera, as described in Fig.1. The planar laser is relatively stationary and coplanar to the reference plate. The planar laser and the plate move in the view-field of the camera. The 3D point $\mathbf{Y}^j$ on the intersection laser stripe is also captured by the camera. The camera coordinate frame (CCF), the image coordinate frame (ICF), and the reference

coordinate frame (RCF) are represented by O^C-$X^CY^CZ^C$, O^D-$X^DY^DZ^D$, and O^O-$X^OY^OZ^O$, respectively.

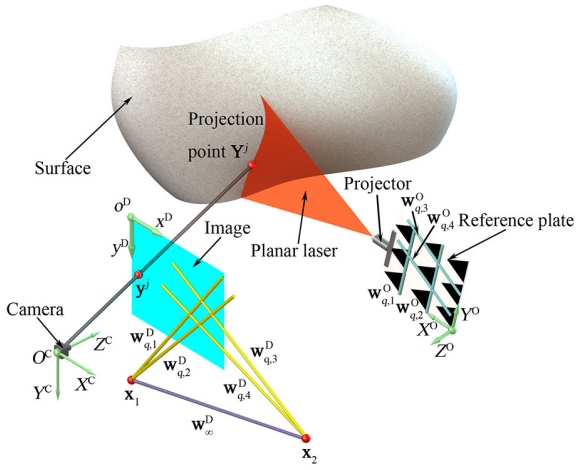

Fig.1. System setup, definitions of the coordinate systems and affine rectification for the active vision reconstruction with the triangle array.

B. Affine rectification

In order to avoid solving the 8 DOFs from the image, the image is affinely rectified by employing a method with the image of the line at infinity in [24]. As the image of the line at infinity can be determined by two pairs of projections of the parallel lines, the parallel-line images are generated from the triangle array pattern and extracted by the Hough transform [25]. A pair of parallel lines intersects at a point at infinity in the image. Thus, two pairs of the parallel lines provide two points at infinity, which determine the line at infinity. In the image, the projections of two pairs of the parallel lines intersect at two points that are the images of the points at infinity. Therefore,

$$\mathbf{x}^{\mathrm{D}}_{q,1} = \mathbf{w}^{\mathrm{D}}_{q,1} \times \mathbf{w}^{\mathrm{D}}_{q,2} \tag{1}$$

$$\mathbf{x}^{\mathrm{D}}_{q,2} = \mathbf{w}^{\mathrm{D}}_{q,3} \times \mathbf{w}^{\mathrm{D}}_{q,4} \tag{2}$$

where $\mathbf{w}^{\mathrm{D}}_{q,1}$, $\mathbf{w}^{\mathrm{D}}_{q,2}$, $\mathbf{w}^{\mathrm{D}}_{q,3}$, $\mathbf{w}^{\mathrm{D}}_{q,4}$ are the images of two pairs of the parallel lines $\mathbf{w}^{\mathrm{O}}_{q,1}$, $\mathbf{w}^{\mathrm{O}}_{q,2}$, $\mathbf{w}^{\mathrm{O}}_{q,3}$, $\mathbf{w}^{\mathrm{O}}_{q,4}$ on the reference plate. The variable q represents the serial number of the q-th parallel line taken in the experiment. The symbol × is the operation of the cross product. $\mathbf{x}^{\mathrm{D}}_{q,1}$, $\mathbf{x}^{\mathrm{D}}_{q,2}$ are the images of the two intersection points of the parallel lines.

As there are several pairs of parallel lines on the reference plate, the images of the points at infinity determine the image of the line at infinity by

$$\left[\left(\mathbf{x}^{\mathrm{D}}_{1,1}\right)^{\mathrm{T}}\left(\mathbf{x}^{\mathrm{D}}_{1,2}\right)^{\mathrm{T}}\left(\mathbf{x}^{\mathrm{D}}_{2,1}\right)^{\mathrm{T}}\left(\mathbf{x}^{\mathrm{D}}_{2,2}\right)^{\mathrm{T}}\cdots\left(\mathbf{x}^{\mathrm{D}}_{q,1}\right)^{\mathrm{T}}\left(\mathbf{x}^{\mathrm{D}}_{q,2}\right)^{\mathrm{T}}\right]^{\mathrm{T}}\mathbf{w}^{\mathrm{D}}_{\infty} = \mathbf{0} \tag{3}$$

where $\mathbf{w}^{\mathrm{D}}_{\infty} = \left[w_1\ w_2\ w_3\right]^{\mathrm{T}}$ is the image of the line at infinity and is determined by the images of the points at infinity. The SVD method [25] is employed to contribute a precise $\mathbf{w}^{\mathrm{D}}_{\infty}$. A pair of infinity points can determine the line at infinity theoretically. However, there are errors in the step of extracting parallel lines from images, which affects the solutions of infinite points and infinite lines. Therefore, we adopt q pairs of points to determine the infinite line jointly, which reduce the impact of noise on the accuracy of the final reconstruction results. As the line at infinity is an invariant for the affine transform, the affine transform from the projection-distortion-image to the affine-distortion-image is $\mathrm{H}=\begin{bmatrix}1&0&0\\0&1&0\\w_1&w_2&w_3\end{bmatrix}$. Therefore, the point in the image with the projection distortion can be transformed to the image with the affine distortion by

$$\mathbf{Y}^{j,\mathrm{F}} = \mathrm{H}\mathbf{y}^{j} \tag{4}$$

where $\mathbf{Y}^{j,\mathrm{F}}$ is the laser point in the affine space with zero value in the vertical axis of the reference. $\mathbf{y}^j$ is the image laser point in the projection space.

C. 3D information solution based on ratio of triangle areas in affine space

After the rectification processed by the line at infinity, there is only the affine distortion in the image. Hence, all the geometrical elements on the plane of the reference plate are transformed in the affine space from the original captured image. In the affine space, centroid and ratio of areas are two invariable features from the original Euclidean space to the affine space [24]. Therefore, the triangle centroid and ratio of triangle areas are selected to determine the information in the Euclidean space by the reference plate with the triangle array, as shown in Fig.2. $\mathbf{X}^i_p$, p = 1, 2, 3, are the centroids of the three small triangles on the reference.

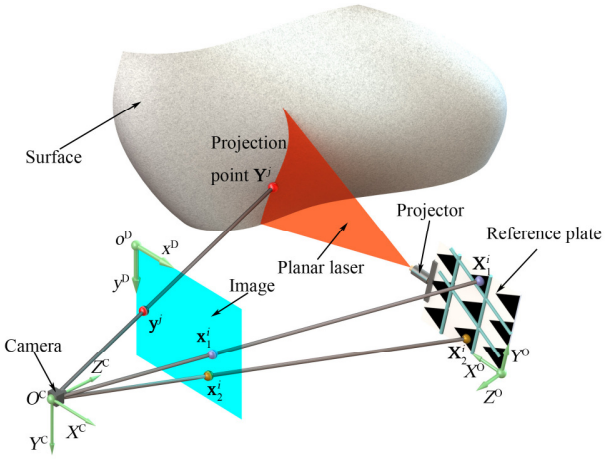

Fig.2. 3D point reconstruction with the ratio of triangle areas in the affine space.

The known vertices of a small triangle on the reference plate are represented by $\mathbf{X}^i_{p,1}$, $\mathbf{X}^i_{p,2}$, $\mathbf{X}^i_{p,3}$ in RCF. $\mathbf{x}^i_{p,1}$, $\mathbf{x}^i_{p,2}$, $\mathbf{x}^i_{p,3}$ are the mapping points of $\mathbf{X}^i_{p,1}$, $\mathbf{X}^i_{p,2}$, $\mathbf{X}^i_{p,3}$ to the image,

respectively. $\mathbf{X}_{p}^{i,\mathrm{F}}$, $\mathbf{X}_{p,1}^{i,\mathrm{F}}$, $\mathbf{X}_{p,2}^{i,\mathrm{F}}$, $\mathbf{X}_{p,3}^{i,\mathrm{F}}$ are the affinely rectified points in the image or, in other words, the points mapped from the original Euclidean space in RCF to the affine space in ICF.

The centroid of the small triangle in RCF is expressed by

$$\mathbf{X}_{p}^{i} = 1/3\left(\mathbf{X}_{p,1}^{i} + \mathbf{X}_{p,2}^{i} + \mathbf{X}_{p,3}^{i}\right) \tag{5}$$

where the variable *i* is the serial number of the element used in the *i*-th area ratio. In the affine space in ICF, the centroid of the small triangle is

$$\mathbf{X}_{p}^{i,\mathrm{F}} = 1/3\left(\mathbf{X}_{p,1}^{i,\mathrm{F}} + \mathbf{X}_{p,2}^{i,\mathrm{F}} + \mathbf{X}_{p,3}^{i,\mathrm{F}}\right) \tag{6}$$

The general affine transform of the vertices of the small triangle from the original Euclidean space in RCF to the affine space in ICF is expressed by

$$\mathbf{X}_{p,1}^{i,\mathrm{F}} = \mathrm{H}_{\mathrm{A}}\mathbf{X}_{p,1}^{i} \tag{7}$$

$$\mathbf{X}_{p,2}^{i,\mathrm{F}} = \mathrm{H}_{\mathrm{A}}\mathbf{X}_{p,2}^{i} \tag{8}$$

$$\mathbf{X}_{p,3}^{i,\mathrm{F}} = \mathrm{H}_{\mathrm{A}}\mathbf{X}_{p,3}^{i} \tag{9}$$

where H_{A} is the affine homography from the original Euclidean space in RCF to the affine space in ICF.

Substitute equations (7)-(9) to equation (6), then

$$\mathbf{X}_{p}^{i,\mathrm{F}} = \mathrm{H}_{\mathrm{A}}\left[1/3\left(\mathbf{X}_{p,1}^{i} + \mathbf{X}_{p,2}^{i} + \mathbf{X}_{p,3}^{i}\right)\right] \tag{10}$$

Stacking equations (5) and (10), the centroid of the small triangle in the affine space is

$$\mathbf{X}_{p}^{i,\mathrm{F}} = \mathrm{H}_{\mathrm{A}}\mathbf{X}_{p}^{i} \tag{11}$$

Therefore, the centroid of the small triangle in the original Euclidean space in RCF is mapped to the corresponding centroid of the small triangle in the affine space.

Note that the points $\mathbf{X}_{p,1}^{i,\mathrm{F}}$, $\mathbf{X}_{p,2}^{i,\mathrm{F}}$, $\mathbf{X}_{p,3}^{i,\mathrm{F}}$ are rectified from the projection space to the affine space by

$$\mathbf{X}_{p,1}^{i,\mathrm{F}} = \mathrm{H}\mathbf{x}_{p,1}^{i} \tag{12}$$

$$\mathbf{X}_{p,2}^{i,\mathrm{F}} = \mathrm{H}\mathbf{x}_{p,2}^{i} \tag{13}$$

$$\mathbf{X}_{p,3}^{i,\mathrm{F}} = \mathrm{H}\mathbf{x}_{p,3}^{i} \tag{14}$$

Moreover, $\mathbf{X}_{p}^{i,\mathrm{F}}$ is derived from equation (6) and equations (12)-(14).

As the ratio of the triangle areas is the invariant of the affine transform, two triangles are generated from the centroids of the small triangles on the reference and the point on the laser stripe. The centroid of the small triangle is selected as an average value of the vertices to minimize the errors. The ratio of two large triangle areas in the original Euclidean space and the affine space is

$$S_{\Delta\mathbf{X}_1^i\mathbf{X}_2^i\mathbf{Y}^j} \Big/ S_{\Delta\mathbf{X}_1^i\mathbf{X}_2^i\mathbf{X}_3^i} = S_{\Delta\mathbf{X}_1^{i,\mathrm{F}}\mathbf{X}_2^{i,\mathrm{F}}\mathbf{Y}^{j,\mathrm{F}}} \Big/ S_{\Delta\mathbf{X}_1^{i,\mathrm{F}}\mathbf{X}_2^{i,\mathrm{F}}\mathbf{X}_3^{i,\mathrm{F}}} \tag{15}$$

where $\mathbf{Y}^{j}$ is the unknown point on the laser stripe in the original Euclidean space. $\mathbf{Y}^{j,\mathrm{F}}$ is the point on the laser stripe in the affine space and is derived from equation (4).

The area of $S_{\Delta\mathbf{X}_1^i\mathbf{X}_2^i\mathbf{Y}^j}$ is solved by equation (15). Let $k^i = S_{\Delta\mathbf{X}_1^i\mathbf{X}_2^i\mathbf{Y}^j}$, $\mathbf{x}_1^i = \left(x_1^i, y_1^i, 1\right)^{\mathrm{T}}$, $\mathbf{x}_2^i = \left(x_2^i, y_2^i, 1\right)^{\mathrm{T}}$, $\mathbf{x}_3^i = \left(x_3^i, y_3^i, 1\right)^{\mathrm{T}}$, $\mathbf{Y}^j = \left(x_4^j, y_4^j, 1\right)^{\mathrm{T}}$. For the *i*-th ratio of the triangle areas, equation (15) is

$$\left(y_1^i - y_2^i\right)x_4^j + \left(x_2^i - x_1^i\right)y_4^j + x_1^i y_2^i - x_2^i y_1^i - 2k^i = 0 \tag{16}$$

Furthermore, for $i = 1, 2, \ldots, n$, equation (16) is arranged to

$$\begin{bmatrix} y_1^1 - y_2^1 & x_2^1 - x_1^1 & x_1^1 y_2^1 - x_2^1 y_1^1 - 2k^1 \\ y_1^2 - y_2^2 & x_2^2 - x_1^2 & x_1^2 y_2^2 - x_2^2 y_1^2 - 2k^2 \\ y_1^3 - y_2^3 & x_2^3 - x_1^3 & x_1^3 y_2^3 - x_2^3 y_1^3 - 2k^3 \\ \cdots & & \\ y_1^n - y_2^n & x_2^n - x_1^n & x_1^n y_2^n - x_2^n y_1^n - 2k^n \end{bmatrix} \begin{pmatrix} x_4^j \\ y_4^j \\ 1 \end{pmatrix} = \mathbf{0}_{n\times 1} \tag{17}$$

where $\mathbf{Y}^j = \left(x_4^j, y_4^j, 1\right)^{\mathrm{T}}$ can be solved by the SVD method [26]. The laser point $\mathbf{Y}^j$ is measured in mm in equation (17). As the method focuses on the recovery of the laser point in Euclidean space, the third degree of the laser point is provided by a ruler rather than the repetition of the point transform to CCF with the well-known Zhang method [27]. Hence, for the experiments, the laser point is represented in RCF.

3. EXPERIMENTS AND DISCUSSION

In the experiments, the instrumentation consists of a 1280×960 resolution camera, a planar laser generator, a ruler, a reference plate patterned with the equilateral triangle array, and a board for the error analysis. The edge length of the triangle is 80 mm. The error analysis board is pasted by the checkerboard pattern and the side length of the element on the board is 30 mm. The planar laser generator is fixed on the reference plate and coplanar with the reference plate. An inspection system composed of a three-dimensional target and a rectangular ruler is designed to verify the coplanarity of the laser plane and the reference plate. Firstly, the 2D reference plate is positioned to be parallel to the bottom plane *O-XY* of the 3D target through the rectangular ruler. The reference plate overlaps the line AB on the *O-XZ* plane of the 3D target. Therefore, the reference plate and the plane ABC are coplanar. Then the laser plane is projected on the target. The laser plane should intersect the *O-YZ* plane of the 3D target with the line BC, or else the laser projector is adjusted by the adjustment screws. Secondly, the 2D reference plate is moved to the other position along the line AB. The intersection laser line between the laser plane and the *O-YZ* plane should also be colinear to the line BC. Thus, the laser plane is coplanar to the plane ABC. Therefore, two

lines on the laser plane are located on the plane ABC which is the same plane of the 2D reference plate. Based on the above process, the laser plane is coplanar to the reference plate. The method and experiment of the coplanarity verification are shown in Fig.3.

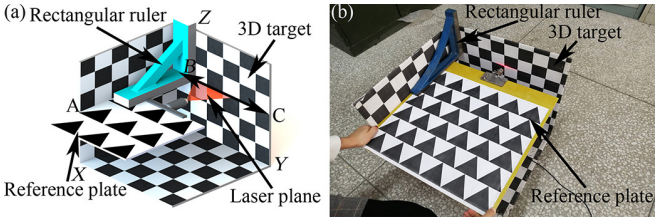

Fig.3. The method and experiment of coplanarity verification of the reference plate and laser plane. a) verification method, b) verification experiment.

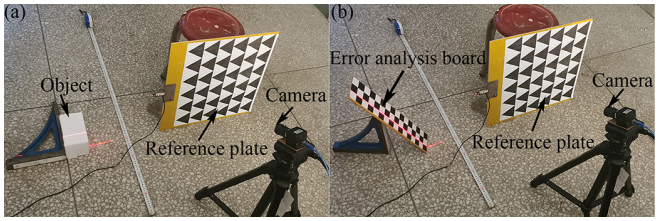

Fig.4. The experimental instruments of the reconstruction based on affine invariability of the ratio of triangle areas. a) object reconstruction, b) error estimation.

Firstly, the camera captures the image of the reference plate. 8 pairs of parallel lines are extracted from the triangle array. The intersection of the line pair, i.e. the image of infinity point, is solved in ICF. Theoretically, only two pairs of parallel lines are enough to determine the image of the line at infinity. However, the accuracy can be improved by appropriately taking multiple groups of parallel lines. Secondly, according to the affine invariability of the ratio of triangle areas, three points on the reference plate are selected to form triangle 1. Each point above is the centroid of a small equilateral triangle, which is more accurate than selecting the vertices of a small triangle as the vertices of triangle 1. Two of the centroids of the small triangles above and a reconstruction point on the intersection laser stripe are chosen to form triangle 2. Then, the affine rectification is performed on the vertex image coordinates of triangle 1 and triangle 2. Finally, the coordinates of the reconstructed points in RCF are obtained from the invariable area ratio. The above reconstruction process is carried out in three groups of triangles, and the results of the three groups are averaged as the final reconstruction results.

A total of six objects are reconstructed in the experiments. The experimental instruments and relative positions are shown in Fig.4.a). The reconstruction results of the six objects are indicated in Fig.5. Fig.5.a) to Fig.5.c), Fig.5.g) to Fig.5.i), and Fig.5.m) to Fig.5.o) are the reconstructed objects. Then, Fig.5.d) to Fig.5.f), Fig.5.j) to Fig.5.l), and Fig.5.p) to Fig.5.r) are the experimental results of the reconstruction method.

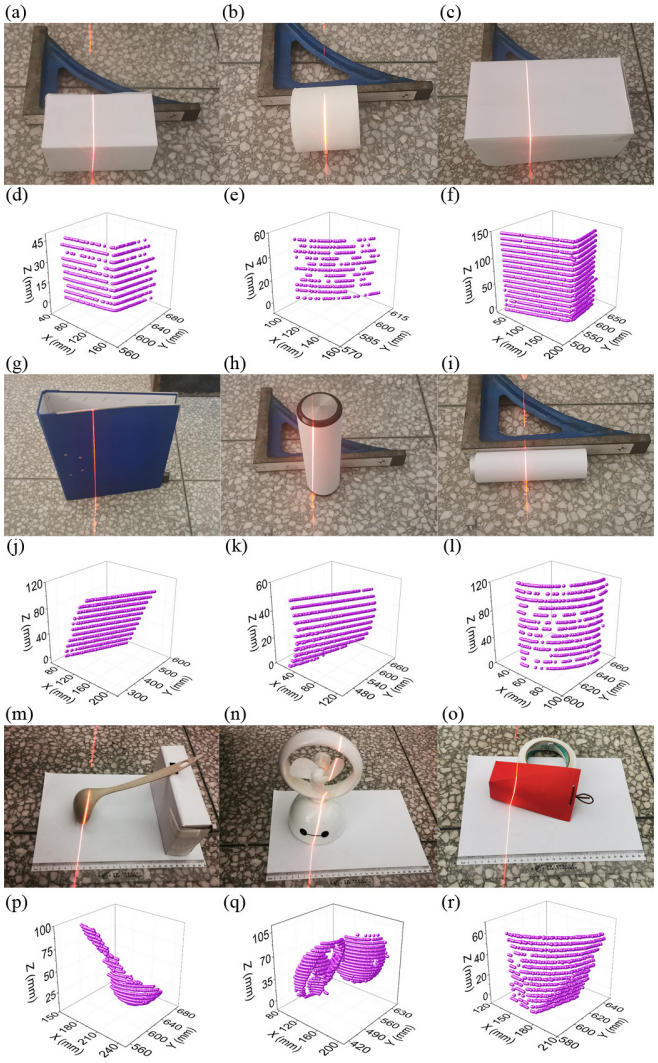

Fig.5. The experimental results of the reconstruction based on the affine invariability of the ratio of triangle areas. a)-c), g)-i) and m)-o) are a gift box, a roll, a snack box, a book holder, a water cup, a bottle, a spoon, a fan and a sugar box. d)-f), j)-l) and p)-r) are the reconstruction results of a)-c), g)-i) and m)-o).

The reconstruction error is estimated and analyzed by the reconstruction experiment of the standard length on the error analysis board. The experimental instruments and relative positions are shown in Fig.4.b). The error value of reconstruction based on the affine invariance of the triangular area ratio is shown in Fig.6. In the test, the reference plate is located on the positions of 550, 600, 650, and 700 mm away from the camera. Four standard lengths of 30, 60, 90, and 120 mm on the error analysis board are selected as the benchmarks. The planar laser is coincident with the reference plate, and the length is then reconstructed in the RCF. The subtraction of the reconstruction length and the standard length accurately describes the reconstruction error. In addition, the error analysis experiments are performed to study the influence of the distance between the error analysis board and the reference plate (DER) on the accuracy. The error analysis board is placed at the positions

of 100, 200, 300, and 400 mm away from the reference plate, respectively. The first set of error tests is conducted by placing the plate at the position 550 mm away from the camera. When the error analysis board is 100 mm away from the reference plate, the error absolute of the system is shown in Fig.6.a). The width of the error bar represents the probability density of the error point, and the shape of the error bar demonstrates the data distribution of the group of the error points. The average reconstruction error of the standard length of 30 mm is 0.99 mm. For the standard length of 60 mm, the error augments to 1.20 mm. For the length of 90 mm, the error rises to 1.40 mm. Finally, when the length is 120 mm, the error is as high as 1.74 mm. The results show that the error tends to increase evidently with the increment of the standard length for the same DER. When the error analysis board is 200, 300, and 400 mm away from the reference plate, the errors for the reference length of 30 mm are 1.10, 1.11, and 1.30 mm, respectively. The results show that the reconstruction error increases slowly with the increment of the DER.

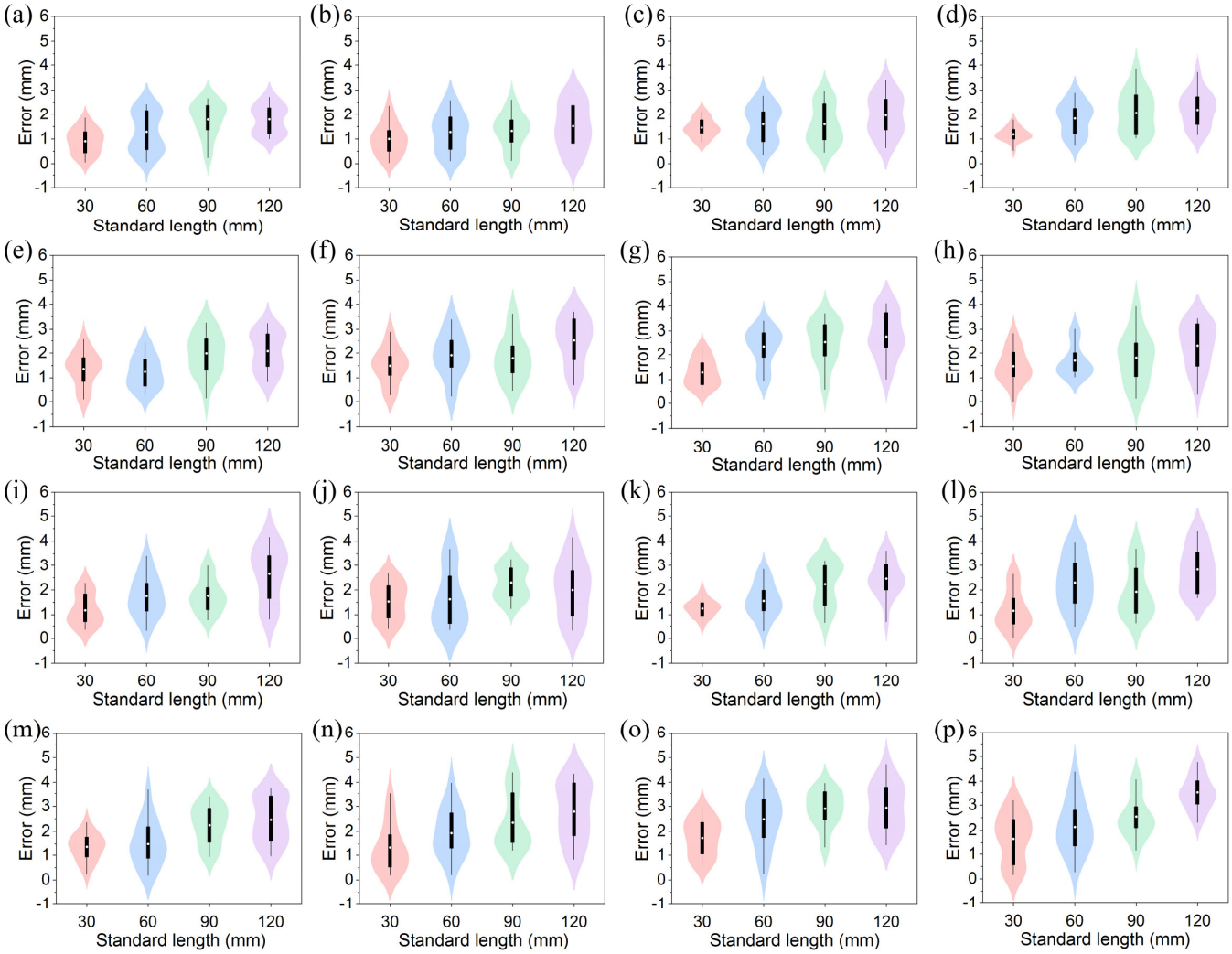

Fig.6. The errors of the reconstruction system based on the affine invariability of the ratio of triangle areas. a)-d) the DRC is 550 mm, the DERs are 100, 200, 300, 400 mm, separately. e)-h) DRC is 600 mm, DERs are 100, 200, 300, 400 mm, separately. i)-l) the DRC is 650 mm, the DERs are 100, 200, 300, 400 mm, separately. m)-p) the DRC is 700 mm, the DERs are 100, 200, 300, 400 mm, separately.

In the next step, the reference plate is placed at distances of 600, 650, and 700 mm away from the camera, and the above experimental process is repeated. When the distance between the reference plate and the camera (DRC) is fixed, the variation law of the reconstruction error is shown in Fig.7. and Table 1. RL is short for the reference length in Table 1. The error analysis experiments are executed to study the impact of DRC on the accuracy, by which the trend of the error can be qualitatively analyzed. The reconstruction error is analyzed by the reconstruction experiment of the standard length on the error analysis board. In the test, four standard lengths of 30, 60, 90, and 120 mm on the error analysis board are selected as the benchmarks. The subtraction result of the reconstruction length and the standard length accurately describes the reconstruction error. The checkerboard pattern on the error

analysis board is printed by Cannon C3020 printer, which provides the printing resolution of 1200 dpi×1200 dpi. As one inch is 25.4 mm, the accuracy of the reference length is 0.02 mm. Furthermore, the reference lengths are also verified by the Vernier caliper. It can be observed from the data in Table 1. that the reconstruction error not only increases significantly as the DER increases, but also increases as the DRC rises. In summary, when the DRC, DER, and reference length are 550, 100, and 30 mm, the reconstruction error approaches a minimum of 0.99 mm.

The experiment is also performed to test and discuss the influence of the number of the parallel lines on the reconstruction error. 3, 4, 5, 6, 7, 8 pairs of the parallel lines are extracted to solve the image of the line at infinity, respectively. Then the reconstruction is carried out based on the different pair number of the parallel lines. The trend of reconstruction errors under all conditions is illustrated in Fig.8. From Fig.8., the accuracy of the method can be refined by appropriately selecting multiple sets of parallel lines.

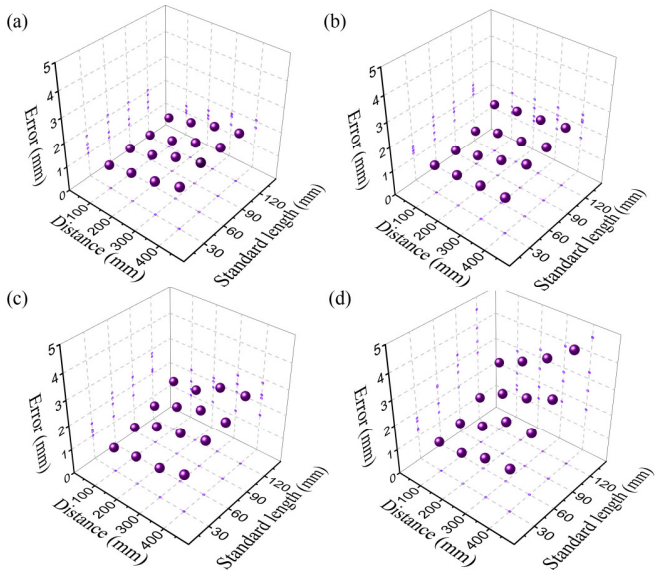

Fig.7. The reconstruction error statistics of the active vision system based on the affine invariability of the ratio of triangle areas. a)-d) the DRCs are 550, 600, 650, and 700 mm, respectively.

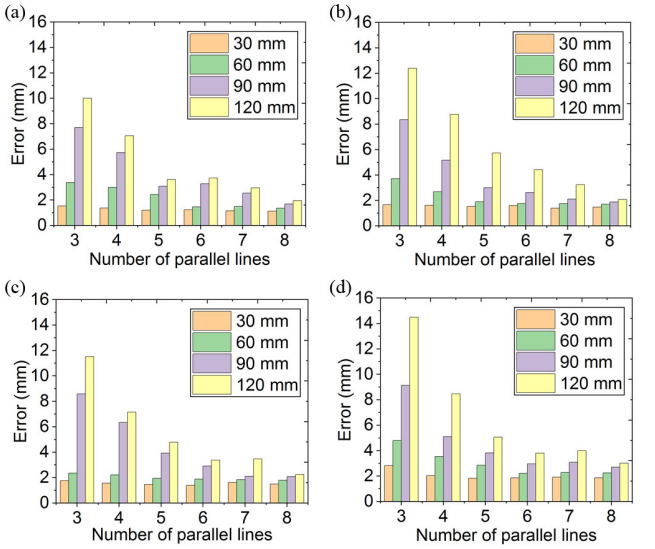

Fig.8. Influence of the different number of parallel lines on the active vision reconstruction based on affine invariability of ratio of triangle areas. a)-d) the DRCs are 550, 600, 650, and 700 mm, separately.

Table 1. The reconstruction error of the method based on the affine invariability of the ratio of triangle areas.

DRC /mm	DER /mm	Error/mm			
		RL= 30	RL= 60	RL= 90	RL= 120
550	100	0.99	1.20	1.40	1.74
	200	1.10	1.34	1.76	2.02
	300	1.11	1.35	1.75	2.04
	400	1.30	1.55	1.86	2.05
600	100	1.18	1.29	1.41	1.49
	200	1.21	1.49	1.81	2.16
	300	1.46	1.84	1.98	2.24
	400	2.05	2.21	2.30	2.45
650	100	1.00	1.16	1.25	1.54
	200	1.26	1.78	2.03	2.23
	300	1.60	2.03	2.36	2.36
	400	2.09	2.18	2.71	2.84
700	100	1.24	1.31	1.64	1.76
	200	1.43	1.80	2.48	2.53
	300	1.95	2.56	2.84	3.24
	400	2.86	3.31	3.84	4.54

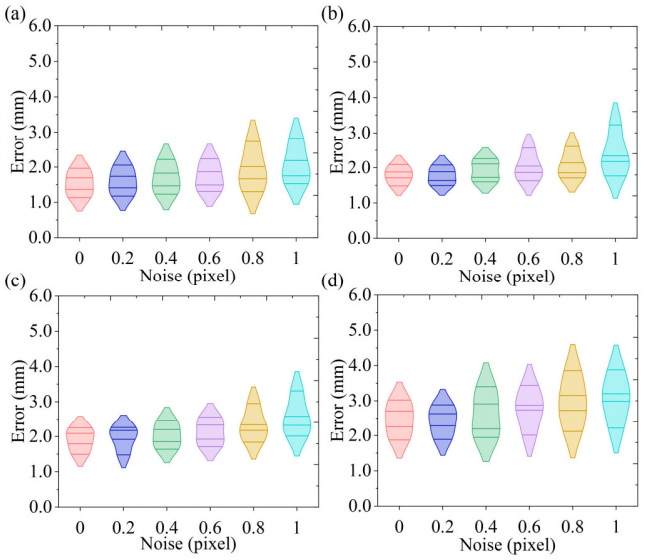

Fig.9. Influence of the image noise on the active vision reconstruction based on affine invariability of the ratio of triangle areas. a)-d) the DRC are 550, 600, 650, 700 mm, separately.

In order to test the influence of the accuracy of the extracted image point coordinates on the reconstruction error, the random Gaussian noise is selected for the extracted point coordinates. Fig.9. shows the variation trend of the reconstruction error under noisy conditions. The random noises with the mean of 0 and the variances of 0.2, 0.4, 0.6, 0.8, and 1.0 pixel are added to the coordinates. The reconstruction error shows a clearly upward trend with the increase of Gaussian noise variance. The mean of the reconstruction errors is 3.07 mm for the noise of 1.0 pixel, DRC of 700 mm.

In order to verify the accuracy of the method, the reconstruction method in Euclidean space [27], and method adopting the small triangle vertices as large triangle vertices are selected for the error comparison test. In the same experimental environment, the reconstruction error derived from the reconstruction distance and the standard distance is tested by the same error analysis board. The comparison results are shown in Fig.10. It can be seen from the error comparison results that the average errors of the three methods increase simultaneously when the DER increases. However, the method in the paper is more stable. When the DER decreases, the reconstruction accuracy of the method in the paper is higher than that of the other two methods.

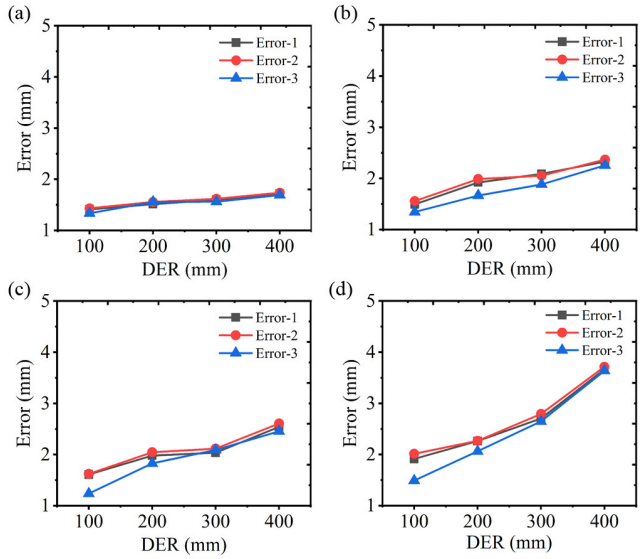

Fig.10. The comparison of average reconstruction errors of three methods. Error-1 is the average error of the method adopting the small triangle vertices as large triangle vertices. Error-2 is the average error of the reconstruction method in Euclidean space. Error-3 is the average error of the reconstruction method in the paper. a)-d) the DRCs are 550, 600, 650, and 700 mm, separately.

4. CONCLUSIONS

This paper proposes an active-vision-based reconstruction method. In the reconstruction model, the planar laser is on the same plane of the reference plate patterned with the equilateral triangle array. The image of the line at infinity is employed to transform the image to the affine space and then the laser point and the centroids of the triangles are adopted to constitute the invariant of the area ratio. According to the affine invariant, the final reconstructed coordinates are obtained in RCF. Since the position of the laser plane can be freely selected, the method is an active vision reconstruction with the high experimental flexibility. Moreover, as the DRC and DER decrease, the reconstruction accuracy will be enhanced. To sum up, the reconstruction method based on the affine invariability of the triangle area ratio has great potential in the field of 3D measurement.

ACKNOWLEDGMENT

This work was supported in part by the National Natural Science Foundation of China under Grants 51875247, 51478204, 51205164 and in part by the Natural Science Foundation of Jilin Province under Grant 20170101214JC.

REFERENCES

[1] Witkovský, V., Frollo, I. (2020). Measurement science is the science of sciences - there is no science without measurement. *Measurement Science Review*, 20 (1), 1-5.

[2] Vrba, I., Palencar, R., Hadzistevic, M., Strbac, B., Spasic-Jokic, V., Hodolic, J. (2015). Different approaches in uncertainty evaluation for measurement of complex surfaces using coordinate measuring machine. *Measurement Science Review*, 15 (3), 111-118.

[3] Timofte, R., Zimmermann, K., Gool, L.J.V. (2014). Multi-view traffic sign detection, recognition, and 3D localisation. *IEEE Workshop on Applications of Computer Vision*, 25 (3), 633-647.

[4] Geiger, A., Lauer, M., Wojek, C., Stiller, C., Urtasun, R. (2014). 3d traffic scene understanding from movable platforms. *IEEE Transactions on Pattern Analysis & Machine Intelligence,* 36 (5), 1012-1025.

[5] Ellekilde, L.P., Huang, S., Jaime, V.M., Dissanayake, G. (2007). Dense 3D map construction for indoor search and rescue. *Journal of Field Robotics*, 24 (1-2), 71-89.

[6] Black, J., Ellis, T. (2002). Multi-camera image measurement and correspondence. *Measurement*, 32 (1), 61-71.

[7] Brosed, F.J., Aguilar, J.J., Guillomia, D., Santolaria, J. (2010). 3D geometrical inspection of complex geometry parts using a novel laser triangulation sensor and a robot. *Sensors,* 11 (1), 90-110.

[8] Mariottini, G.L., Scheggi, S., Morbidi, F., Prattichizzo, D. (2012). Planar mirrors for image-based robot localization and 3-D reconstruction. *Mechatronics*, 22 (4), 398-409.

[9] Mikulka, J. (2015). GPU-accelerated reconstruction of T2 maps in magnetic resonance imaging. *Measurement Science Review*, 15 (4), 210-218.

[10] Dvořák, P., Bartušek, K., Smékal, Z. (2014). Unsupervised pathological area extraction using 3D T2 and FLAIR MR images. *Measurement Science Review*, 14 (6), 357-364.

[11] Samper, D., Santolaria, J., Brosed, F.J., Aguilar, J.J. (2013). A stereo-vision system to automate the manufacture of a semitrailer chassis. *International Journal of Advanced Manufacturing Technology,* 67 (9-12), 2283-2292.

[12] Geng, J. (2011). Structured-light 3D surface imaging: A tutorial. *Advances in Optics and Photonics*, 3 (2), 128-160.

[13] Hu, X., Mordohai, P. (2012). A quantitative evaluation of confidence measures for stereo vision. *IEEE Transactions on Pattern Analysis and Machine Intelligence,* 34 (11), 2121-2133.

[14] Chen, G., Guo, Y., Wang, H., Ye, D., Gu, Y. (2012). Stereo vision sensor calibration based on random spatial points given by CMM. *Optik - International Journal for Light and Electron Optics,* 123 (8), 731-734.

[15] Li, T., Almond, D.P., Rees, D.A.S. (2011). Crack imaging by scanning pulsed laser spot thermography. *Ndt & E International*, 44 (2), 216-225.

[16] Vilaca, J.L., Fonseca, J.C., Pinho, A.M. (2009). Calibration procedure for 3D measurement systems using two cameras and a laser line. *Optics and Laser Technology*, 41 (2), 112-119.

[17] Salvi, J., Pages, J., Batlle, J. (2004). Pattern codification strategies in structured light systems. *Pattern Recognition,* 37 (4), 827-849.

[18] Orghidan, R., Salvi, J., Gordan, M., Florea, C., Batlle, J. (2014). Structured light self-calibration with vanishing points. *Machine Vision & Applications*, 25 (2), 489-500.

[19] Guillou, E., Meneveaux, D., Maisel, E., Bouatouch, K. (2000). Using vanishing points for camera calibration and coarse 3D reconstruction from a single image. *The Visual Computer*, 16 (7), 396-410.

[20] Wang, L., Tsai, W. (1991). Camera calibration by vanishing lines for 3-D computer vision. *IEEE Transactions on Pattern Analysis & Machine Intelligence,* 13 (4), 370-376.

[21] Zhao, Y., Lv, X.D. (2012). An approach for camera self-calibration using vanishing-line. *Information Technology Journal*, 11 (2), 276-282.

[22] Gibbs, G.A., Pound, M., French, A., Wells, D., Murchie, E., Pridmore, T. (2019). Active vision and surface reconstruction for 3D plant shoot modelling. *IEEE/ACM Transactions on Computational Biology & Bioinformatics*.

[23] Schacter, D.S., Donnici, M., Nuger, E., Mackay, M., Benhabib, B. (2014). A multi-camera active-vision system for deformable-object-motion capture. *Journal of Intelligent & Robotic Systems,* 75 (3-4), 413-441.

[24] Hartley, R., Zisserman, A. (2004). *Multiple View Geometry in Computer Vision*. Cambridge University Press.

[25] Mukhopadhyay, P., Chaudhuri, B.B. (2015). A survey of Hough transform. *Pattern Recognition*, 48 (3), 993-1010.

[26] Horn, R.A., Johnson, C.R. (2012). *Matrix Analysis.* Cambridge University Press.

[27] Zhang, Z.Y. (2000). A flexible new technique for camera calibration. *IEEE Transactions on Pattern Analysis and Machine Intelligence*, 22 (11), 1330-1334.

Received March 18, 2020
Accepted August 17, 2020